Imaging Tumor-Stroma Interactions during Chemotherapy Reveals Contributions of the Microenvironment to Resistance

Elizabeth S. Nakasone,[1,2,10] Hanne A. Askautrud,[1,3,4,5,10] Tim Kees,[1] Jae-Hyun Park,[1] Vicki Plaks,[3] Andrew J. Ewald,[3,6] Miriam Fein,[1,7] Morten G. Rasch,[1,8] Ying-Xim Tan,[3] Jing Qiu,[1] Juwon Park,[1] Pranay Sinha,[1] Mina J. Bissell,[9] Eirik Frengen,[4,5] Zena Werb,[3,11] and Mikala Egeblad[1,3,11,*]
[1]Cold Spring Harbor Laboratory
[2]Watson School of Biological Sciences
Cold Spring Harbor, NY 11724, USA
[3]Department of Anatomy, University of California, San Francisco, San Francisco, CA 94143, USA
[4]Department of Medical Genetics, Institute of Clinical Medicine, University of Oslo, N-0315 Oslo, Norway
[5]Department of Medical Genetics, Oslo University Hospital, N-0424 Oslo, Norway
[6]Departments of Cell Biology and Oncology, Center for Cell Dynamics, Johns Hopkins School of Medicine, Baltimore, MD, 21205, USA
[7]Graduate Program in Genetics, Stony Brook University, Stony Brook, New York 11794, USA
[8]Finsen Laboratory, Copenhagen University Hospital, DK-1165 Copenhagen, Denmark
[9]Life Sciences Division, Lawrence Berkeley National Laboratory, Berkeley, CA 94720, USA
[10]These authors contributed equally to this work
[11]These authors contributed equally to this work
*Correspondence: egeblad@cshl.edu
DOI 10.1016/j.ccr.2012.02.017

SUMMARY

Little is known about the dynamics of cancer cell death in response to therapy in the tumor microenvironment. Intravital microscopy of chemotherapy-treated mouse mammary carcinomas allowed us to follow drug distribution, cell death, and tumor-stroma interactions. We observed associations between vascular leakage and response to doxorubicin, including improved response in matrix metalloproteinase-9 null mice that had increased vascular leakage. Furthermore, we observed CCR2-dependent infiltration of myeloid cells after treatment and that *Ccr2* null host mice responded better to treatment with doxorubicin or cisplatin. These data show that the microenvironment contributes critically to drug response via regulation of vascular permeability and innate immune cell infiltration. Thus, live imaging can be used to gain insights into drug responses in situ.

INTRODUCTION

One of the major challenges in treating cancer is resistance to therapy. It is well appreciated that cancer cell intrinsic factors, such as genetic or epigenetic changes, can cause development of therapy resistance (Dean et al., 2005). Extrinsic factors in the microenvironment of certain organs, such as the bone marrow and thymus, can also confer resistance (Gilbert and Hemann, 2010; Meads et al., 2009). In these cases, resistance is mediated by factors secreted from stromal cells, such as IL-6. In addition,

impaired drug penetration through the extracellular matrix (ECM) influences drug response in primary solid tumors (Loeffler et al., 2006; Olive et al., 2009).

Surprisingly little is known about how cells in intact tumors respond to classical chemotherapies (Minchinton and Tannock, 2006; Rottenberg et al., 2010). Most of the knowledge about these responses has been obtained from cell culture or xenograft experiments, where cancer cells grow under conditions very different from the microenvironment of human tumors. Indeed, such experiments are often not predictive of drug

Significance

It is well appreciated that intrinsic factors regulate chemoresponsiveness. Using in vivo microscopy of tumors, we show that extrinsic factors within the microenvironment support the development of chemoresistance by regulating drug distribution and the inflammatory response. These results have clinical implications, as myeloid cell infiltration is increased in human breast tumors after chemotherapy and the cellular composition of the immune infiltrate is a strong predictor of overall survival. Our data suggest that the response to classical chemotherapeutic drugs can be improved by changing the tumor microenvironment with agents that modify matrix metalloproteinase activity and chemokine signaling. Our study shows that observing the tumor response in real-time at cellular resolution can yield insights into the biology of chemoresistance.

responses in patients (Johnson et al., 2001; Minchinton and Tan-nock, 2006).

To investigate the role of the microenvironment in chemo-sponsiveness, we chose a well-documented mouse model, the mammary tumor virus (MMTV) promoter-driven polyoma middle T oncogene (PyMT) model, that displays progressive stages of tumorigenesis similar to human luminal type B breast cancer (Herschkowitz et al., 2007; Lin et al., 2003). As MMTV-PyMT tumors progress, cancer cells undergo molecular changes, including increased expression of ErbB receptor family members (Lin et al., 2003). In parallel, the stromal microenviron-ment undergoes changes in blood vessel architecture, ECM composition, and immune cell infiltration (Egeblad et al., 2008, 2010).

RESULTS

Doxorubicin Induces Necrotic Cell Death In Vivo
Doxorubicin (Adriamycin) is a cytotoxic drug used to treat advanced breast cancer (Rouzier et al., 2005). To investigate the acute, cellular response to doxorubicin treatment in the context of the tumor microenvironment, we monitored mammary carcinomas in live mice using spinning disk confocal microscopy (Egeblad et al., 2008). MMTV-PyMT mice were crossbred with the ACTB-ECFP and c-fms-EGFP reporter mice to enable visualization of different tumor stages and tracking of the most abundant stromal cell type, myeloid cells (Egeblad et al., 2008). Dead cells were labeled with propidium iodide (PI) administered intraperitoneally (i.p.). Cell death became apparent 24–30 hr after doxorubicin administration and increased as imaging continued, whereas there was limited cell death in untreated control mice (Figure 1A; Figure S1A available online; see Figure 2 for quantifi-cation). The death of individual cells was readily observed as the appearance of PI staining (Figure 1B; Movie S1). In addition to cell death in the tumor mass, we observed stromal cell death (Figure 1A).

Necrosis is a major pathway of cell death after doxorubicin treatment in vitro (Obeid et al., 2007). Cell death by apoptosis and necrosis are characterized by specific changes in nuclear morphology and plasma membrane integrity (Dive et al., 1992). We next determined the nature of doxorubicin-induced cell death in vivo by imaging changes in nuclear morphology in MMTV-PyMT;ACTB-ECFP mice crossbred with mice expressing histone H2B conjugated to EGFP (Hadjantonakis and Papaioan-nou, 2004). The majority of the nuclei became positive for PI before their morphology changed, indicating early loss of plasma membrane integrity and necrosis-like cell death. A small percentage of cells died with breakdown of chromatin into condensed bodies followed by acquisition of PI labeling, indi-cating late loss of plasma membrane integrity and apoptosis-like cell death (Figures 1C and 1D; Movie S2). By histology, we observed only a minor increase in the number of cells with the condensed chromatin that is typical of apoptosis after doxoru-bicin treatment (Figure S1B). Thus, doxorubicin predominantly induces necrosis in vivo.

Doxorubicin Sensitivity Changes with Tumor Stage
At the macroscopic level, doxorubicin treatment reduced tumor volume in MMTV-PyMT mice bearing multiple tumors (Figures

2A and S2A). However, the smallest or largest tumors tended to be resistant (Figure S2B), suggesting that resistance was associated with tumor progression.

MMTV-PyMT tumors have been classified into four patholog-ical stages, based on cellular morphology, lack of basement membrane, and infiltration of immune cells (Lin et al., 2003). We adapted this classification to allow a simplified assess-ment of tumor stage in live animals: "hyperplasia," small lesions showing increased accumulation of cells as compared to normal epithelium; "early carcinoma," lesions with evidence of myeloid cell infiltration and/or cancer cell invasion; and "late carcinoma," large lesions with densely packed cancer cells (Egeblad et al., 2008). MMTV-PyMT mammary glands have multiple tumors, which are often at different stages of progression. This allowed us to image doxorubicin response at different stages in the same mouse (Figures 2B and S2C). Cell death increased after doxorubicin-treatment in early carci-nomas (Figure 2C); on average, 10% of the fields of view (FOV) were positive for PI at 31 hr after doxorubicin-treatment compared to 2% of the FOV in the controls (Figure S2D). In contrast, cell death did not increase in hyperplasias and late carcinomas after treatment (Figures 2B, 2C, S2C, and S2D; Movie S3), suggesting marked differences in drug sensitivity between tumor stages. Cancer cells in early carcinomas also accumulated more DNA damage after doxorubicin treatment than those in hyperplasias or late carcinomas, as determined by immunostaining for histone γ-H2AX (Figure 2D). Thus, doxorubicin sensitivity changes with tumor stage but not in a linear manner.

Cancer Cell Proliferation Does Not Correspond to Doxorubicin Sensitivity In Vivo
Doxorubicin intercalates into DNA, inhibiting topoisomerase II. Hence, proliferating cells are predicted to be more sensitive than resting cells (Campiglio et al., 2003). Yet, cancer cell prolif-eration differed insignificantly between tumor stages (Figure 2E). Furthermore, in pulse-chase experiments, the percentage of dead cells that were BrdU$^+$ was similar in doxorubicin- and phos-phate buffered saline (PBS)-treated tumors (Figure 2F). These data suggest that differences in cellular proliferation between tumor stages are not the main cause of differences in doxoru-bicin sensitivity in vivo.

Primary Cancer Cells from Different Tumor Stages Do Not Exhibit Intrinsic Differences in Doxorubicin Sensitivity in Culture
As tumors progress, cancer cells acquire mutations and silence or activate genes. These changes can give rise to differences in sensitivity between tumor stages. To distinguish the contribution of cancer cell intrinsic changes from those of the tissue microen-vironment, we isolated cancer cells from MMTV-PyMT; ACTB-ECFP mice using a fluorescent dissection microscope. This allowed us to visualize the cancer epithelium during tissue removal, ensuring that tumors were representative of the different stages (Figure S2E). Indeed, in vitro sensitivity to the ErbB1/ErbB2 inhibitor lapatinib was highest for cells isolated from late carcinomas (Figure 2G), as predicted from the increased expression of the ErbB2/Neu oncoprotein in late-stage tumors (Lin et al., 2003). In contrast, cells from hyperplasia,
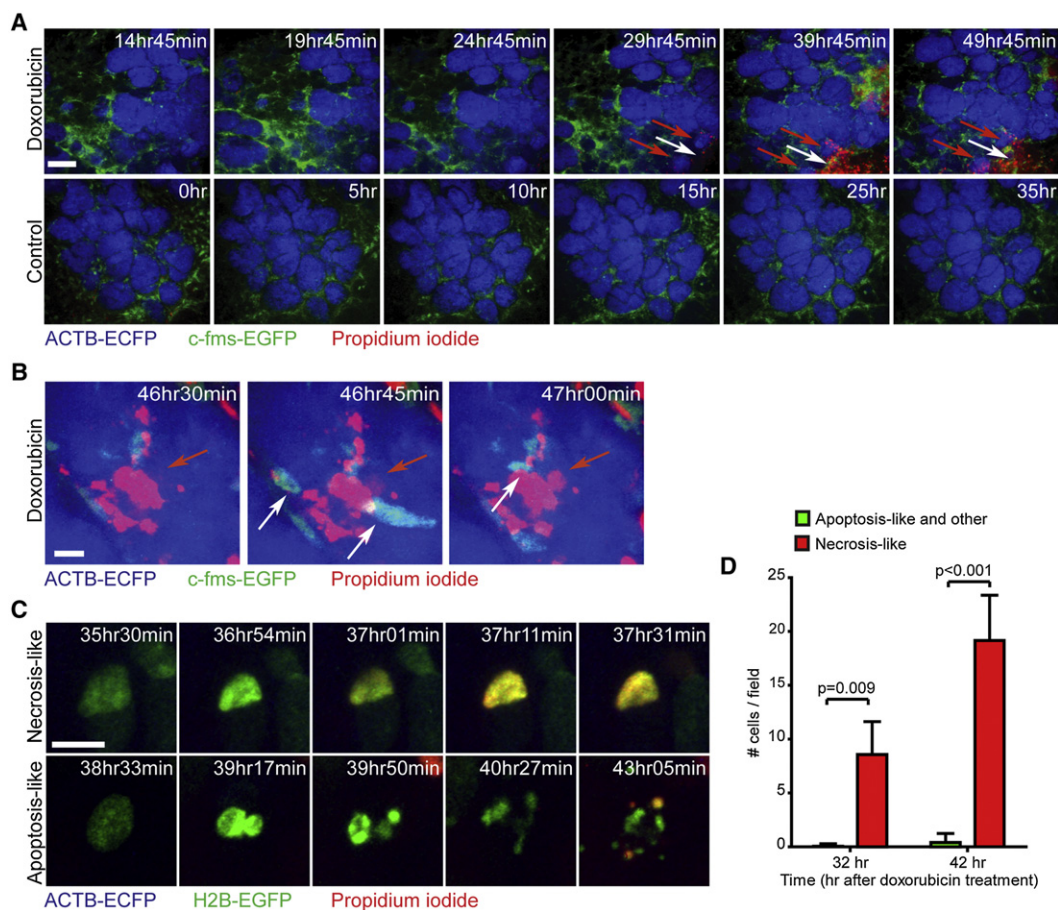
Figure 1. Visualizing Cellular Responses to Chemotherapy In Vivo

(A) Doxorubicin-induced cell death in tumors of live MMTV-PyMT;ACTB-ECFP;c-fms-EGFP mice. Induction of cell death (red), visualized by propidium iodide (PI) uptake, can be seen in a tumor lesion (blue) infiltrated with myeloid cells (green). Red arrows point to cell death in the tumor, and white arrows point to cell death in the stroma. Time after treatment (doxorubicin) or initiation of imaging (control) is indicated. Scale bar: 100 μm.

(B) Dynamics of cell death in situ. Single cell death was observed as the appearance of PI staining (red arrow). This was followed by myeloid cell infiltration (white arrows). Time after doxorubicin treatment is indicated. Scale bar: 10 μm.

(C) Dynamics and types of nuclear structural changes after doxorubicin treatment in MMTV-PyMT;ACTB-ECFP;H2B-EGFP mice. Examples of necrosis-like (nucleus becomes PI[+] without major structural changes) and apoptosis-like (nuclear structure breakdown before PI uptake) cell death. Time after treatment is indicated. Scale bar: 10 μm.

(D) Doxorubicin induces necrosis-like cell death (mean ± SEM; 18 fields of view [FOV] from three mice were counted; $p = 0.009$ at 32 hr, $p < 0.001$ at 42 hr, Student's t test).

Also see Figure S1 and Movies S1 and S2.

early carcinoma, and late carcinoma stages had similar sensitivity to doxorubicin in both two- and three-dimensional cultures (Figures 2H, 2I, and S2F). Primary macrophages and the macrophage cell line RAW 264.7 were also sensitive to doxorubicin (Figure S2G), in accordance with the stromal cell death observed by imaging. Taken together, the in vitro data indicated that cancer cell intrinsic mechanisms are unlikely to be responsible for the differences in doxorubicin sensitivity that were observed between tumor stages and that extrinsic mechanisms are operative in vivo.

Visualization of Drug Distribution in Real-Time Reveals Its Association with Drug Response

Interstitial fluid pressure is one extrinsic factor that increases in late-stage tumors as compared to early stages and it

hinders drug penetration into tumors (Hagendoorn et al., 2006; Netti et al., 1999). Therefore, we hypothesized that differences in drug response between tumor stages might be related to differences in drug accessibility. Doxorubicin is naturally fluorescent, allowing for imaging of its distribution. However, its broad emission and excitation spectra overlap with those of our fluorescent reporters. It was therefore not possible to image doxorubicin distribution in MMTV-PyMT; ACTB-ECFP mice in which tumor stage could be determined. Instead, we imaged unlabeled MMTV-PyMT mice and identified tumor areas by palpation and abnormal tumor vasculature, visualized using intravenously (i.v.) injected fluorescent nanoparticles (AngioSPARK 680).

We imaged small (just palpable), medium (~160 mm³), and large (~845 mm³) tumors (Figure 3A; Movies S4 and S5).

Doxorubicin rapidly leaked out into the tissue and accumulated in the nuclei of cells near blood vessels (Figure 3A). This resulted in an intravascular half-life of 9.5 min (range, 7.9–11.8 min; Figure 3B), consistent with the initial plasma half-life of 8.5 min (range, 7.2–9.8 min) reported in human patients (Greene et al., 1983). Doxorubicin distribution varied among tumors of different sizes (Figures 3A and 3C), with the most leakage in larger tumors and the least leakage in those that were just palpable. Furthermore, significantly more doxorubicin was extractable from small tumors (13–81 mm^3) than from hyperplastic MMTV-PyMT tissues or normal mammary glands (Figure 3D). Solid tumors tend to have progressed further than softer ones, and when tumors were analyzed based on consistency, as well as size, the highest levels of doxorubicin were found in soft tumors, although the values were not significantly higher than in solid tumors of similar size (Figure 3E).

Tumor size and consistency is not an accurate indicator of tumor stage. Thus, to quantify vascular leakage in tumors of different stages, we co-injected i.v. fluorescent 10 kD (low) and 2 MD (high) molecular mass dextrans into MMTV-PyMT;ACTB-ECFP mice (Figures 4A and S3A; Movie S6). The intravascular half-lives of dextrans were similar in tumor microenvironments at different stages (Figures S3B and S3C), with a higher intravascular half-life for 2 MD dextran (41 [range, 32–58] min) than for 10 kD dextran (15 [range, 14–16] min; Figure S3D).

In contrast to intravascular half-life, leakage of dextrans into the extravascular space and their retention in tissues were clearly influenced by tumor stage (Figures 4A and 4B). Regions with hyperplasias showed limited leakage into the extravascular space, whereas early carcinomas and the tumor-stroma borders of late carcinomas exhibited substantially more leakage. Extravasated 10 kD dextran reached a larger area of the tissue than did extravasated 2 MD dextran (Figures 4A and 4B). Following extravasation, the dextrans accumulated in stromal cells, which we have previously shown are c-fms$^+$CD68$^+$CD206$^+$ macrophages (Egeblad et al., 2008). Leakage in normal mammary glands was minimal and below detection limits when the settings used for tumor-bearing mice were applied (not shown).

Finally, we co-injected i.v. doxorubicin-treated mice with 10 kD dextran and *Ricinus communis* agglutinin I, a lectin that binds to basement membrane exposed to the vascular lumen, marking leaky vasculature (Thurston et al., 1999). We observed that only tumor areas in close proximity to these two markers contained cells with nuclear uptake of doxorubicin (Figure S3E). Interestingly, some of the cells with doxorubicin-positive nuclei had also taken up dextran, suggesting that they were macrophages (Figure S3E).

Absence of MMP9 Results in Increased Vascular Leakage and Sensitizes Tumors to Doxorubicin Treatment

Tumor-associated macrophages promote vascular changes (Egeblad et al., 2010). We found that the extent of local c-fms-EGFP$^+$ myeloid cell infiltration correlated significantly with the degree of local 10 kD dextran leakage, regardless of tumor stage (Figures 4C and 4D). Myeloid cells can regulate vessel stability via secretion of vascular endothelial growth factor (VEGF) and transforming growth factor (TGF)-β, both of which are seques-

tered in the ECM and released by matrix metalloproteinases (MMPs; Yu and Stamenkovic, 2000; Ebrahem et al., 2010). Nevertheless, MMPs may also negatively regulate vascular permeability (Sounni et al., 2010). Several MMPs, including MMP9, are expressed at high levels by tumor-infiltrating myeloid cells (Figure 5A). To determine if host-derived MMP9 affects vascular stability and doxorubicin response, we transplanted MMTV-PyMT cancer cells to wild-type FVB/n and *Mmp9*$^{-/-}$ hosts and treated them with doxorubicin. Although MMP9 does not influence primary tumor growth in the transgenic MMTV-PyMT model (Martin et al., 2008), we found that the growth of grafted tumors was reduced in *Mmp9*$^{-/-}$ hosts compared to FVB/n hosts (Figure S4A). Interestingly, tumors in *Mmp9*$^{-/-}$ hosts responded better to doxorubicin than those in FVB/n hosts (Figure S4B).

Since transplanted MMTV-PyMT tumors grew slower in *Mmp9*$^{-/-}$ hosts, we could not rule out that the influence of MMP9 on doxorubicin response was related to its effects on cancer cell proliferation. Therefore, we tested if MMP9 influenced the response in the MMTV-Neu model, another doxorubicin-sensitive, luminal breast cancer model, in which the absence of MMP9 does not affect cancer cell proliferation or tumor growth (Figures S4C and S4D; data not shown). Vascular volume, determined by i.v. tomato lectin staining, was not affected by MMP9 status, but tumor vessels were leakier in the absence of MMP9, as determined by i.v. staining with *Ricinus communis* agglutinin I (Figures 5B–5D). In the absence of MMP9, the endothelial cell adhesion molecule VE-cadherin showed increased phosphorylation (Figures 5E and 5F), which results in loose adherence junctions (Gavard, 2009). Vascular coverage with pericytes, which support endothelial cells, was also decreased (Figures 5G and S4E). In keeping with the increased permeability of the vasculature, MMTV-Neu;*Mmp9*$^{-/-}$ tumors treated with doxorubicin responded better than did MMTV-Neu;*Mmp9*$^{+/+}$ tumors (Figure 5H). In contrast, C3(1)-Tag tumors, a basal-like mammary carcinoma model that is largely doxorubicin-resistant (Figure S4F), did not respond better in the absence of MMP9 (Figure S4G).

Doxorubicin Treatment Leads to Recruitment of Myeloid Cells to Tumors

We observed that vascular leakage was associated with higher infiltration of macrophages (Figure 4D), so we sought to determine the effect of MMP9 on macrophage infiltration. There were increased numbers of cells expressing the F4/80 and CD206 macrophage markers in untreated tumors of *Mmp9*$^{-/-}$ hosts compared to those of FVB/n hosts (Figures 6A and 6B). Interestingly, doxorubicin treatment significantly reduced the number of macrophages in *Mmp9*$^{-/-}$ hosts, suggesting that macrophages were killed.

Despite the reduction in macrophage numbers observed after doxorubicin-treatment of *Mmp9*$^{-/-}$ hosts, imaging consistently showed recruitment of myeloid cells to doxorubicin-treated tumors in wild-type mice (Figures 6C and 6D; Movie S7). These myeloid cells often formed granuloma-like structures in areas with cell death (Movie S7). Rarely, we observed myeloid cell recruitment prior to cancer cell death (Figure S5A).

Myeloid cells are a diverse family of innate immune cells, including neutrophils, monocytes, and macrophages, that are
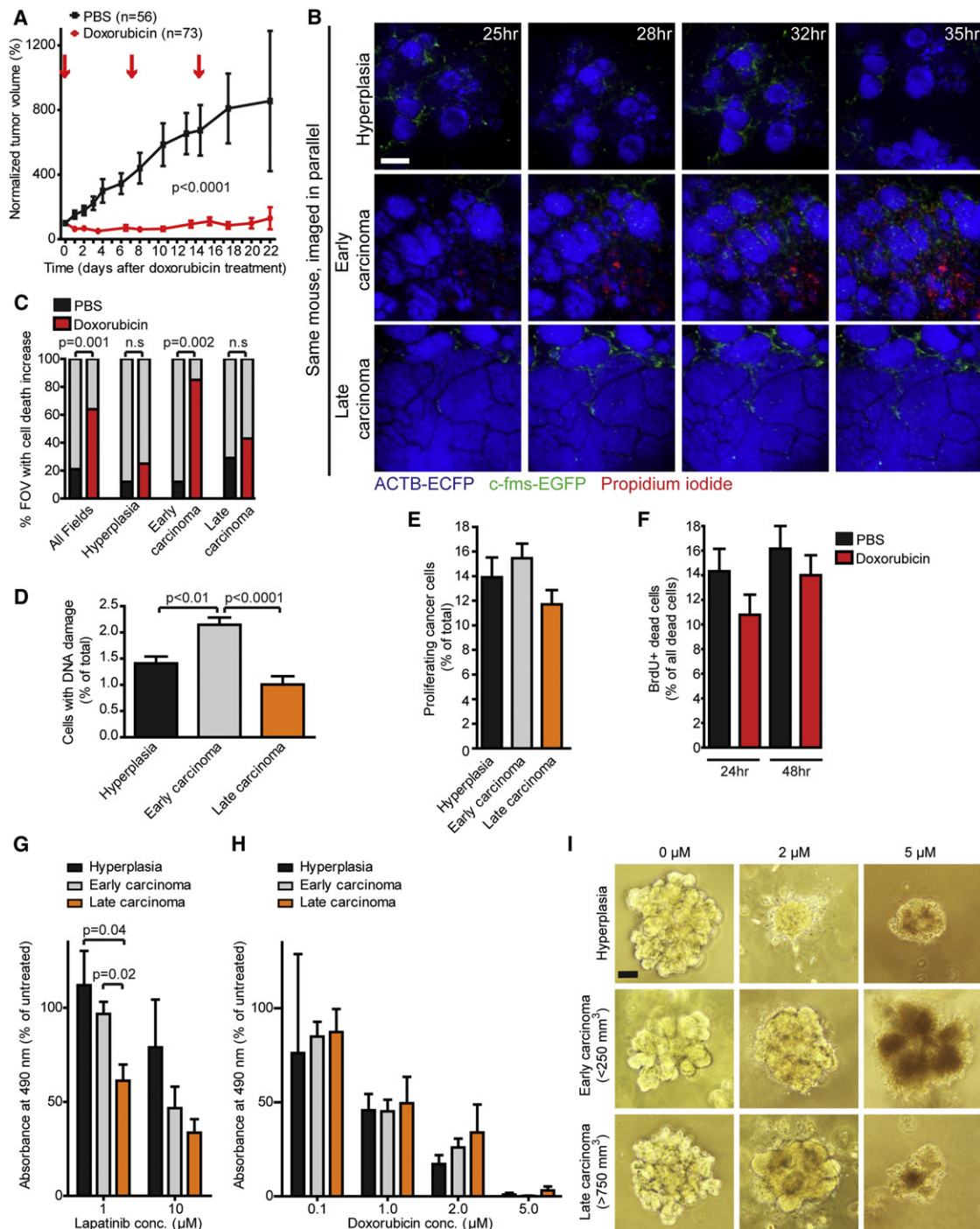
Figure 2. Doxorubicin Sensitivity Changes with Tumor Stage In Vivo but Not In Vitro

(A) Doxorubicin treatment reduces tumor volume in MMTV-PyMT mice. Mice were given doxorubicin or PBS at days 0, 7, and 14 (indicated by arrows). Analysis includes 73 tumors from eleven doxorubicin-treated mice and 56 tumors from 12 PBS-treated mice (mean ± SEM, p < 0.0001 for all time-points, Student's t test).

(B) Doxorubicin-induced cell death preferentially occurs in early carcinomas and not in hyperplasias and late carcinomas. Different microenvironments imaged in the same MMTV-PyMT;ACTB-ECFP;c-fms-EGFP mouse after doxorubicin treatment. Time after treatment is indicated. Scale bar: 100 μm.

(C) Cell death increases between 24 and 36 hr after doxorubicin treatment (n = 25 fields of view [FOV]) as compared to control mice imaged for similar time frames (n = 23 FOV; Fisher's exact test; p = 0.001). Cell death increases in early carcinomas (12 of 14 doxorubicin-treated versus 1 of 8 control-treated FOV, Fisher's exact test, p = 0.002) but not in hyperplasias (1 of 4 versus 1 of 8 fields) or late carcinomas (3 of 7 versus 2 of 7). Four control- and four doxorubicin-treated mice were imaged.

(D) DNA damage response measured by γ-H2AX immunostaining differs between tumor stages (mean ± SEM, analysis of variance [ANOVA], p < 0.0001) and is higher in early carcinomas than in hyperplasia (p < 0.01, Bonferroni posttest) or late carcinomas (p < 0.0001; Bonferroni posttest; 21 hyperplasia, 25 early carcinoma, and 24 late carcinoma FOV were evaluated in five tumors from five mice).

all recruited to areas of cell death (Murdoch et al., 2004). To determine a basis for myeloid cell infiltration, we injected necrotic cell debris into mammary glands of non-tumor-bearing mice and imaged the response. In this model, the results are independent of any direct effects of doxorubicin on myeloid cells, such as induction of cell death. Myeloid cell infiltration increased in areas injected with necrotic debris as compared to areas injected with only saline and dextran (Figure S5B). Once a myeloid cell recognized the cell debris, other myeloid cells were rapidly recruited and a granuloma-like structure was formed (Figure S5B; Movie S8). Myeloid cell recruitment is often mediated by G_i-protein-coupled chemokine receptors (Sadik et al., 2011). Mice pretreated with pertussis toxin, a G_i-protein inhibitor, showed reduced myeloid cell recruitment to cell debris, suggesting the involvement of chemokine receptors in this process (Figure S5C; Movie S9).

Myeloid Cells Are Recruited to Doxorubicin-Treated Tumors through a Stromal CCL2/CCR2 Chemokine/ Chemokine Receptor Axis

To screen for candidate chemokines involved in the recruitment of myeloid cells, we used a protein array. Tumor lysates isolated 48 hr after doxorubicin treatment showed increased protein levels for CCL2 and CCL12 (Figure 7A). Both of these chemokines are ligands for the CCR2 receptor, which is expressed on monocytes and is responsible for their recruitment to sites of inflammation (Tsou et al., 2007). We also observed small increases in macrophage colony-stimulating factor (M-CSF/CSF1) and tissue inhibitor of metalloproteinase 1 (TIMP1; Figure 7A). We confirmed the increases in CCL2 and CCL12 by enzyme-linked immunosorbent assay and immunostaining (Figures 7B, S6A, and S6B). CCL2-expressing cells were large cells located in the stroma that did not express markers of fibroblasts and pericytes (Figure 7C) or endothelial cells (Figure 7D).

Next, we investigated the types of myeloid cells recruited after doxorubicin treatment. Infiltration of cells expressing a neutrophil/monocyte marker, the 7/4 antigen (Ly6B.2), was significantly increased (Figure 7E). This increase was exclusively found among cells that also expressed the CCL2 receptor, CCR2, and had a monocytic nuclear morphology (Figures 7E and S6C). The number of $7/4^+CCR2^-$ cells did not increase but rather decreased, after doxorubicin treatment (Figure 7E). A small number of $CCR2^+$ cells did not express the 7/4 antigen, but their numbers did not change after doxorubicin treatment (Figure 7E). In contrast to the acute increase in the infiltration of $7/4^+CCR2^+$ cells, overall macrophage infiltration, as determined by the F4/80 marker, was not changed 48 hr after doxo-

rubicin treatment (Figure S6D). However, a small increase was seen in the number of cells within the tumor mass that expressed CD206, a marker of alternatively activated macrophages (Figure S6E).

We next tested whether CCR2 mediates the myeloid cell infiltration seen after doxorubicin treatment. We transplanted primary cancer cells isolated from MMTV-PyMT mice to $Ccr2^{-/-}$ or C57BL/6 hosts and characterized the myeloid cell population after doxorubicin treatment. In C57BL/6 hosts, the fraction of cells co-expressing the myeloid cell marker CD11b with the monocyte/neutrophil markers Gr1 and 7/4 increased significantly after doxorubicin treatment (Figures 7F and 7G). The total proportion of cells in the tumors that expressed the myeloid CD11b marker did not increase (Figure S6F). Tumors of $Ccr2^{-/-}$ hosts had a higher fraction of $CD11b^+7/4^+Gr1^+$ cells than did C57BL/6 hosts (Figures 7F and 7G), consistent with previous reports (Pahler et al., 2008). However, there was no significant increase in this cell population after doxorubicin treatment in $Ccr2^{-/-}$ hosts (Figures 7F and 7G). Doxorubicin treatment did not affect the subpopulations of $CD11b^+$ cells that expressed F4/80 or CXCR4 in either genotype (Figures S6G—S6I). Together, our results suggest that doxorubicin treatment leads to a specific, acute recruitment of CCR2-expressing myeloid cells of the monocytic lineage through stromally expressed CCL2.

Host CCR2 Influences Tumor Response to Chemotherapy

To determine if CCR2-mediated recruitment of myeloid cells influenced the response to doxorubicin, we generated cohorts of MMTV-PyMT;$Ccr2^{+/-}$ and MMTV-PyMT;$Ccr2^{-/-}$ mice. For doxorubicin-sensitive tumors (250–750 mm^3), the absence of CCR2 was associated with a significantly better response, although tumors in both cohorts ultimately relapsed (Figure 8A). In contrast, tumors below 250 mm^3, which respond poorly to doxorubicin, did not show a better response to treatment when mice were deficient for CCR2 (Figure S7A).

CCL2 has been proposed to promote cancer cell survival through CCR2 receptors on cancer cells (Zhang et al., 2010). To rule out the involvement of CCR2 signaling in cancer cells, we transplanted primary cancer cells from MMTV-PyMT mice to $Ccr2^{-/-}$ or C57BL/6 hosts. When treated with doxorubicin or cisplatin, a different class of chemotherapeutic drug with efficacy against MMTV-PyMT tumors (Figure S7B), tumors in $Ccr2^{-/-}$ hosts relapsed later than those in C57BL/6 hosts (Figures 8B and 8C). Tumor growth before treatment was not significantly different between $Ccr2^{-/-}$ and C57BL/6 hosts (Figure 8B). Myeloid cells can secrete factors that increase cancer

---

(E) Cancer cell proliferation determined by BrdU labeling does not differ between tumor stages in MMTV-PyMT mice (mean ± SEM, not significant, n.s., ANOVA; 13 hyperplasia, 19 early carcinoma, and 28 late carcinoma FOV were evaluated in six tumors from three mice).

(F) Proliferating ($BrdU^+$) cells are not preferentially killed by doxorubicin treatment. The fraction of $BrdU^+$ cells with cell death-associated nuclear changes was scored (mean ± SEM, n.s., Student's t test; for each condition, 58–60 FOV were analyzed in six tumors from three mice).

(G) Sensitivity to the ErbB1/ErbB2 inhibitor lapatinib is highest for cancer cells from late-stage tumors in culture (mean ± SEM, p = 0.04 or 0.02 as indicated, Student's t test; values represent the averages of four experiments, each done in triplicate with primary cells from independent mice).

(H) Sensitivity to doxorubicin is not affected by tumor stage in culture (mean ± SEM, n.s., ANOVA; values represent the averages of four experiments, each done in triplicate with primary cells from independent mice).

(I) Morphology of organoids generated from tumors at different stages after treatment with the indicated concentrations of doxorubicin. Scale bar: 50 μm.
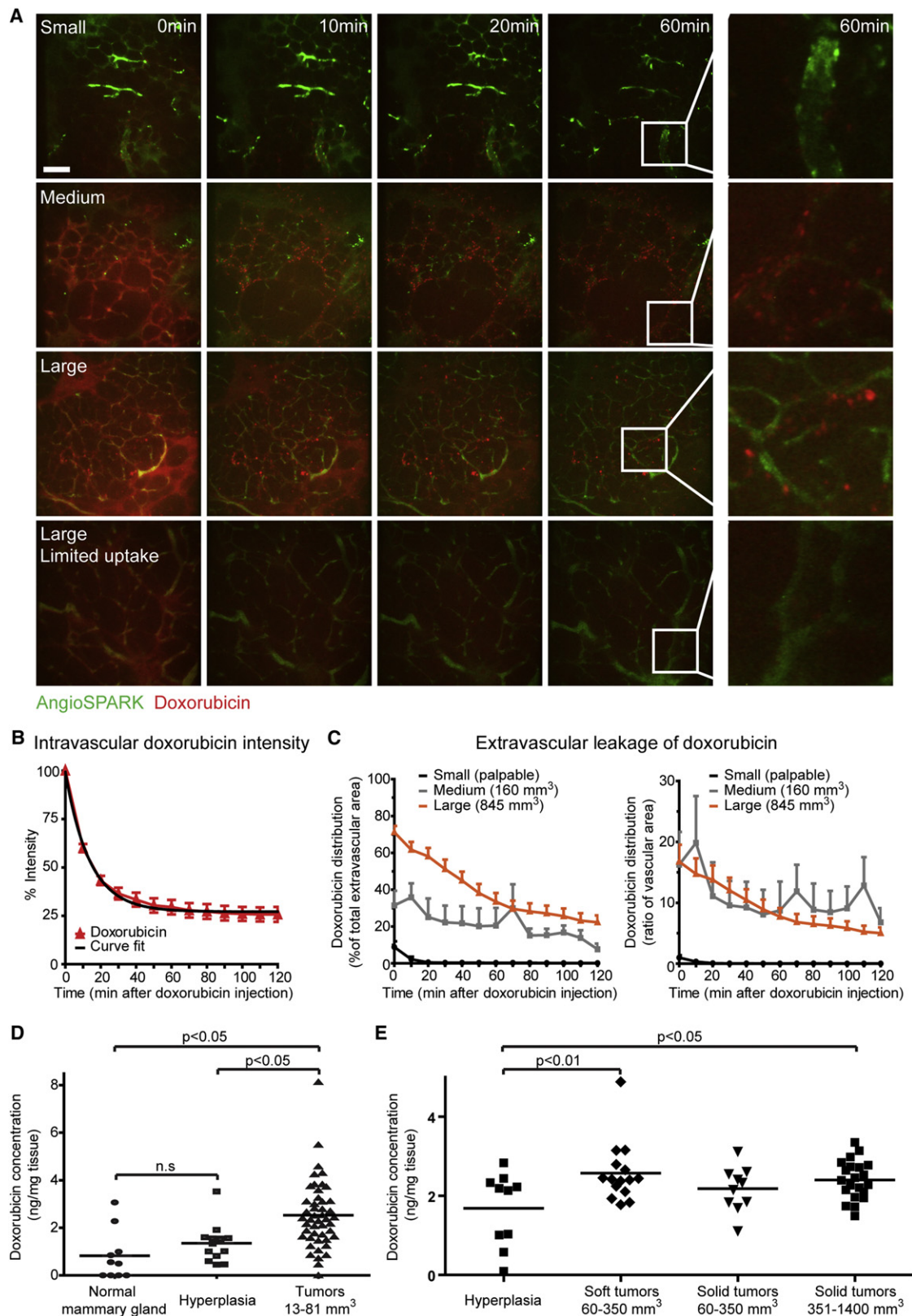
Also see Figure S2 and Movie S3.

Figure 3. Distribution and Uptake of Doxorubicin in Different Tumor Sizes
(A) Doxorubicin leakage and uptake vary with tumor size. MMTV-PyMT mice with small (just palpable tumors), medium (~160 mm³), or large tumors (~845 mm³) were injected intravenously with AngioSPARK 680 (green) and doxorubicin (red). Minimal leakage and uptake were seen in small tumors. Leakage was high in

cell survival (Shree et al., 2011). However, we detected no lasting survival benefit on primary cancer cells when they were cultured with primary macrophages (Figures S7C and S7D).

Although tumors in $Ccr2^{-/-}$ hosts relapsed, they were of a strikingly lower histological grade than the high-grade relapsed tumors of C57BL/6 hosts (Figure 8D). Histological differences were already evident 48 hr after doxorubicin treatment as tumors in $Ccr2^{-/-}$ hosts were more cystic than those in C57BL/6 hosts (Figure 8D). Taken together, our data suggest that infiltration of CCR2-expressing myeloid cells into chemotherapy-treated tumors contributes to tumor regrowth after treatment.

Like CCR2, MMP9 can also influence myeloid cell recruitment (Gong et al., 2008). We therefore tested whether the effects of MMP9 on doxorubicin response could be explained by effects on the acute recruitment of myeloid cells to treated tumors. However, adaptively transferred bone marrow cells from c-fms-EGFP;$Mmp9^{+/+}$ and c-fms-EGFP;$Mmp9^{-/-}$ mice were recruited equally well to tumors of MMTV-PyMT mice after treatment with doxorubicin (Figure S7E). Next, we tested whether the changed myeloid cell environment in $Ccr2^{-/-}$ mice correlated with vascular changes, akin to the effects of loss of $Mmp9$ (Figure 8E). Whereas the vascular volume was higher in tumors of $Ccr2^{-/-}$ mice (Figure 8F), the percentage that was leaky was significantly lower, with the net result being no change in the total volume of leaky vasculature (Figures 8G and 8H). Furthermore, pericyte coverage of the vasculature was increased in $Ccr2^{-/-}$ hosts, whereas VE-cadherin phosphorylation levels were unaffected (Figures S7F–S7I). Thus, although the response to doxorubicin is improved in both $Mmp9^{-/-}$ and $Ccr2^{-/-}$ microenvironments, the effects on vascular structure and myeloid cell recruitment after treatment are different.

DISCUSSION

We imaged the dynamics of doxorubicin responses in a progressive cancer model and revealed that chemosensitivity in vivo is influenced by the tumor microenvironment. The highest sensitivity to doxorubicin was not observed in the earliest or latest tumor stages but rather in the intermediate stage. These differences in drug response between stages were associated with parallel differences in vascular leakage. We therefore tested doxorubicin response in $Mmp9$ null tumor microenvironments with increased vascular permeability and found an improved response. Doxorubicin treatment led to the recruitment of $CCR2^+$ monocytic cells to tumors. In $Ccr2$ null microenviron-

ments, recruitment was inhibited and the response to chemotherapy better. These results have clinical implications, as myeloid cell infiltration is increased in human breast tumors after chemotherapy and the composition of the immune infiltrate is a predictor of survival (Denardo et al., 2011).

Stromal Regulation of Vascular Leakage

Primary cancer cells from different stages responded similarly to doxorubicin in vitro, whereas doxorubicin sensitivity, tumor stage, and vascular leakage were related in vivo. This suggests that stage-specific changes in vascular leakage contributed to doxorubicin response although we cannot exclude contributions from stromal cells. Strikingly, increased leakage of the tumor vasculature in $Mmp9^{-/-}$ mice corresponded to a better response to doxorubicin. The increased vascular permeability in $Mmp9^{-/-}$ mice was associated with decreased pericyte-coverage of the vasculature and increased phosphorylation of VE-cadherin, which affect endothelial cell-cell adhesions (Gavard, 2009; Goel et al., 2011). Although MMP inhibitors have failed in clinical trials (Coussens et al., 2002), our data suggest that these, or other drugs that affect vascular permeability, could be used to achieve better responses to chemotherapies.

MMP9 may regulate vascular structure by acting on a substrate in the tumor microenvironment. Indeed, a reduction of infiltrating $MMP9^+$ myeloid cells through inhibition of the CSF-1 receptor results in a better response to anti-VEGFR2 treatment (Priceman et al., 2010). However, MMP9 may also regulate vascular permeability indirectly through its effects on macrophage infiltration. Macrophages can secrete VEGF (also known as vascular permeability factor), which induces VE-cadherin phosphorylation in endothelial cells (Gavard, 2009).

Myeloid cells are not the only stromal cells capable of regulating drug delivery in tumors. By decreasing the fibroblast pool, and thus the ECM, drugs better enter the tissue (Loeffler et al., 2006; Olive et al., 2009). Interestingly, the improved drug delivery in these cases is achieved by increased vascular density and "vascular normalization," which involves better pericyte coverage and reduced permeability (Goel et al., 2011). Since vascular volume and pericyte coverage increased in tumors of $Ccr2^{-/-}$ compared to C57BL/6 hosts, such vascular changes could play a role in the MMTV-PyMT model. Untangling the roles of MMP9 and CCR2 on vasculature, myeloid cell infiltration, and drug response will require the ability to temporally and conditionally manipulate these genes.

---

medium and some large tumors, with variable nuclear retention. Time after doxorubicin injection is indicated. The last column shows nuclear uptake of doxorubicin (higher magnification of the areas outlined in the fourth column). Scale bar: 100 μm.

(B) Decay of intravascular doxorubicin levels determined by imaging is modeled as one-phase exponential decay (black line; mean ± SEM; eight FOV from two mice were analyzed).

(C) Kinetics of doxorubicin leakage from vessels in tumors of different sizes. Quantification of the percentage of extravascular pixels with doxorubicin signal above intensity threshold (150% of background) and as a ratio of extravascular doxorubicin to vascular area (mean ± SEM; eight small, four medium, and eleven large FOV were analyzed in six mice).

(D) Doxorubicin concentration is higher in tumors than hyperplasias and normal mammary glands (means are shown; $p < 0.0001$, ANOVA, and Bonferroni posttests for comparison of groups; $p < 0.05$ or n.s. as indicated; ten normal mammary glands from five FVB/n mice and 14 hyperplastic and 47 tumors [13–81 mm^3] from five MMTV-PyMT were analyzed).

(E) Doxorubicin concentration is higher in tumors that were soft upon dissection than in hyperplastic tissue or solid tumors of similar size (means are shown, $p = 0.01$, ANOVA, and Bonferroni posttests for comparison of groups; $p < 0.01$ or 0.05 as indicated). Ten hyperplastic, 15 soft and medium-sized (60–350 mm^3), ten solid and medium-sized (60–350 mm^3), and 21 solid and large tumors (351–1,400 mm^3) from five MMTV-PyMT mice were analyzed.

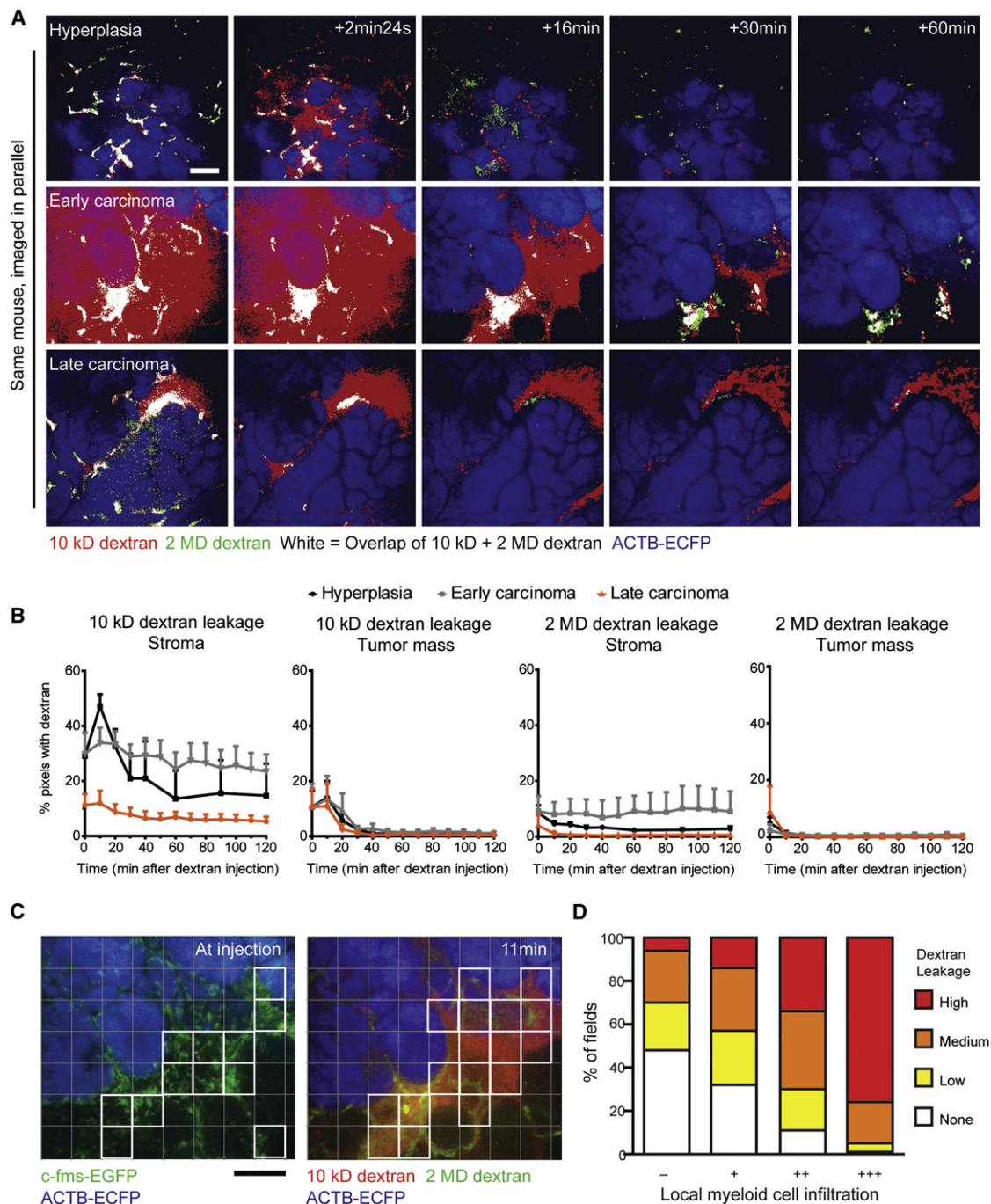Also see Movies S4 and S5.

Figure 4. Leakage and Distribution of Intravenously Injected Dextran Varies with Tumor Stage

(A) Early carcinomas exhibit a higher degree of dextran leakage than do hyperplasias and late carcinomas. More extensive leakage of 10 kD than 2 MD dextran is shown for all tumor stages. Kinetics of 10 kD (red) and 2 MD dextran (green) leakage from vessels in three different tumor stages from the same MMTV-PyMT; ACTB-ECFP mouse are shown. Regions with leakage of both dextrans are depicted in white and the epithelium in blue (ACTB-ECFP). Time after dextran injection is indicated. Scale bar: 100 μm.

(B) Quantification of the percentage of pixels above intensity threshold (150% of background) for the two dextrans in the epithelial and stromal compartments (mean ± SEM; four hyperplasias from two mice, five early carcinomas from four mice, and five late carcinomas from four mice were analyzed).

(C) The extent of c-fms-EGFP+ myeloid cell infiltration in MMTV-PyMT;ACTB-ECFP;c-fms-EGFP mice and the degree of 10 kD dextran leakage were scored independently using the indicated pixel grid. Co-injected 2 MD dextran was used to differentiate between intra- and extravascular 10 kD dextran. Examples of pixel fields scored as maximal infiltration and leakage are indicated by the white boxes. Scale bar: 100 μm.

(D) Myeloid cell infiltration correlates with dextran leakage (r = 0.56 and r = 0.47, for observer A and B, respectively, p < 0.0001, Spearman's rank correlation coefficient; 720 FOV from two mice were scored).
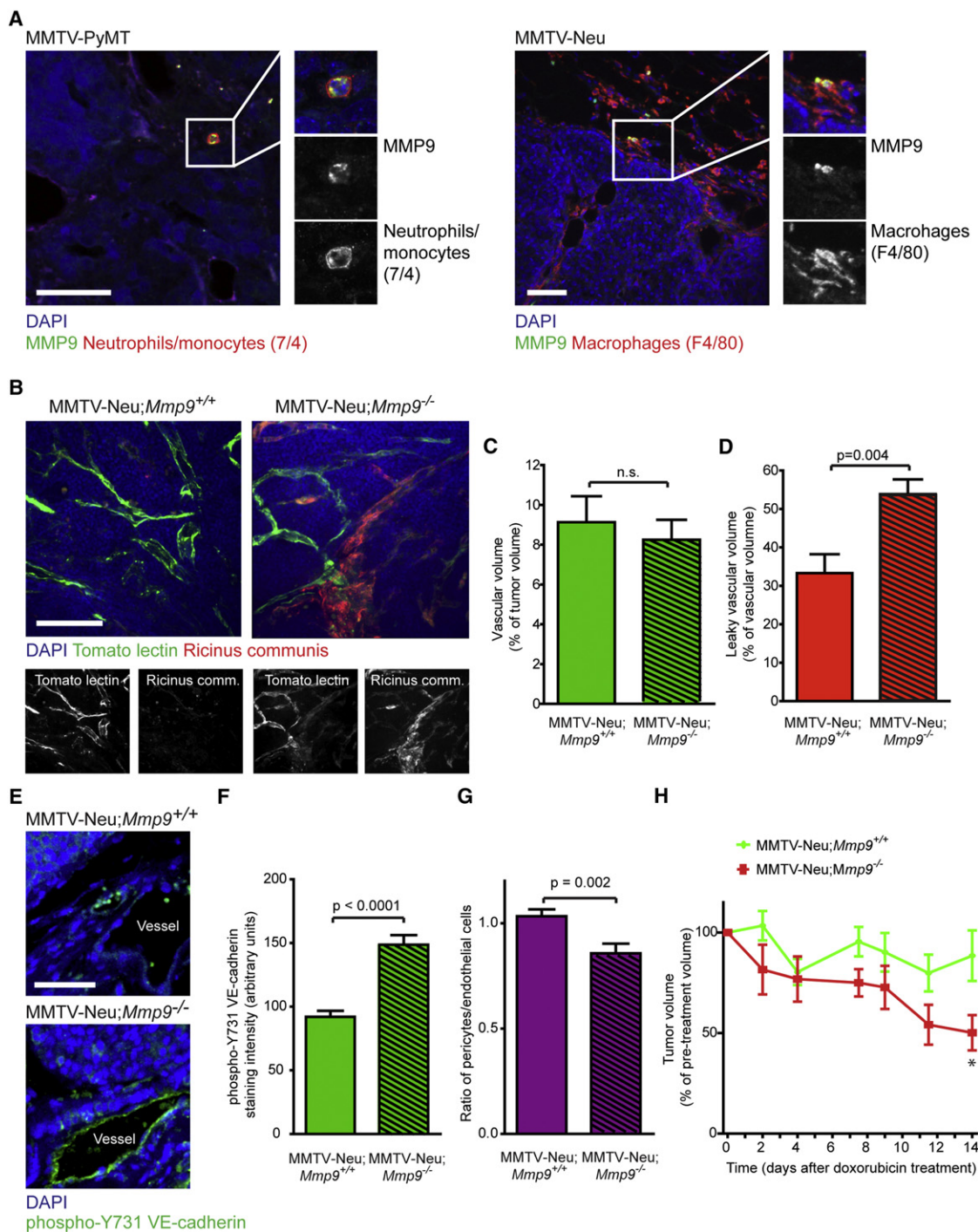
Also see Figure S3 and Movie S6.

Figure 5. Matrix Metalloproteinase-9 Is Expressed by Myeloid Cells and Influences Vascular Leakage and Response to Doxorubicin

(A) MMP9 is expressed by tumor-infiltrating myeloid cells, including those marked by 7/4 (neutrophils/monocytes) and F4/80 (macrophages). Scale bars: 50 μm.

(B) Vascular structure of tumors in MMTV-Neu;$Mmp9^{+/+}$ and MMTV-Neu;$Mmp9^{-/-}$ mice analyzed by perfusion with FITC-conjugated tomato lectin (green, labels all blood vessels) and rhodamine-conjugated *Ricinus communis* agglutinin I (red, labels basement membrane exposed to the vascular lumen in leaky vessels). Scale bar: 100 μm.

(C) Vascular volume as determined by perfusion with tomato lectin does not differ between MMTV-Neu;$Mmp9^{+/+}$ and MMTV-Neu;$Mmp9^{-/-}$ mice (mean ± SEM, n.s., Student's t test, 33 FOV in ten tumors from five MMTV-Neu;$Mmp9^{+/+}$ mice and 29 FOV in eight tumors from three MMTV-Neu;$Mmp9^{-/-}$ mice were analyzed).

(D) Blood vessels are leakier in MMTV-Neu;$Mmp9^{-/-}$ tumors. The percentage of the vasculature that is positive for *Ricinus communis* agglutinin I is shown (mean ± SEM, p = 0.004, Student's t test, 33 FOV in ten tumors from five MMTV-Neu;$Mmp9^{+/+}$ mice and 29 FOV in eight tumors from three MMTV-Neu;$Mmp9^{-/-}$ mice were analyzed).

(E) Immunostaining for phospho-Y731 VE-cadherin. Scale bar: 100 μm.

The Role of Myeloid Cell Recruitment in Chemotherapy Responses

Recruitment of CCR2^{+} monocytes after doxorubicin treatment correlated with tumor relapse. Similarly, an increased number of macrophages is found after treatment of tumors with chemotherapy and is associated with poor drug response (Denardo et al., 2011; Shree et al., 2011). Such macrophages can promote cancer cell survival through the secretion of cysteine cathepsins (Shree et al., 2011). CCR2^{+} monocytes could be the source of tumor-associated macrophages in the posttreatment microenvironment. Indeed, we did not observe increased numbers of macrophages 48 hr after treatment, whereas they have been observed 7–12 days after the first dose of chemotherapy in the MMTV-PyMT model (Denardo et al., 2011; Shree et al., 2011). However, macrophage infiltration depends on CSF-1 (Denardo et al., 2011). Furthermore, macrophages do not promote survival of cancer cells in a cathepsin-dependent manner after treatment with the cisplatin-related drug carboplatin (Shree et al., 2011), whereas the response to cisplatin was better in $Ccr2^{-/-}$ hosts. Thus, it is possible that CCR2^{+} monocytes and tumor-associated macrophages are recruited through independent pathways and influence drug responses through independent mechanisms. Several such mechanisms likely exist. For example, Tie-2-expressing macrophages are recruited after hypoxic tissue injury through a CXCL12/CXCR4 chemokine axis (Welford et al., 2011).

Our results, as well as those of others (Ahn et al., 2010; Denardo et al., 2011; Shree et al., 2011; Welford et al., 2011), indicate that the myeloid cell infiltration that occurs after chemotherapy, radiation, or tissue injury impedes the response to therapy. However, myeloid cell recruitment can also lead to the direct killing of cancer cells (Guerriero et al., 2011), thereby increasing the response to chemotherapy. These differences in the effects of recruited myeloid cells are likely due to the recruitment of different subpopulations of myeloid cells. Indeed, infiltration of CD206^{+} macrophages was associated with increased vascular leakage and better doxorubicin response, whereas reduced CCR2-dependent recruitment of monocytic cells was associated with delayed tumor relapse.

Interestingly, stromal cells expressed CCL2 after doxorubicin treatment. This offers a possible explanation for the observation that stromally derived, but not cancer cell-derived, CCL2 is associated with decreased relapse-free survival in breast cancer patients (Fujimoto et al., 2009). Furthermore, administration of antibodies specific for mouse CCL2 enhances the response to docetaxol in a xenograft model of prostate cancer (Loberg et al., 2007).

Conclusions

In vivo imaging of tumors shows that different components of the microenvironment participate in the development of chemoresistance. Disruption of these microenvironments is beneficial for the response to doxorubicin and cisplatin. Our data suggest that existing drugs that inhibit MMPs or chemokine signaling may be effective when combined with traditional chemotherapies. However, the order and timing of administration of such combination therapies could be critical because of the complexity of the interactions between myeloid cells and vasculature in chemotherapy responses. Future studies combining imaging with molecular approaches hold promise for gaining further insights into the targeting of tumors in the context of its microenvironment.

EXPERIMENTAL PROCEDURES

Animals

MMTV-PyMT (FVB/n), MMTV-Neu (FVB/n), ACTB-ECFP (FVB/n), ACTB-H2B-EGFP (obtained on mixed background and backcrossed to FVB/n for six generations), and $Ccr2^{-/-}$ (C57BL/6) mice were from Jackson Laboratory. MMTV-PyMT (C57BL/6) mice were provided by Dr. Kasper Almholt, and c-fms-EGFP mice were provided by Dr. Jeffrey Pollard and backcrossed to FVB/n mice for six generations. $Mmp9^{-/-}$ mice (FVB/n) were previously described (Vu et al., 1998). All animal experiments were conducted in accordance with procedures approved by the IACUC at Cold Spring Harbor Laboratory or the University of California, San Francisco.

Tumor Transplantation Experiments

Virgin females of 6–16 weeks of age were used as hosts for transplantation. Cancer cells were isolated from 2–3 tumors at 8–10 mm diameter from MMTV-PyMT mice. Tumors were mechanically dissociated and digested with collagenase (0.2% w/v), trypsin (0.2% w/v), and DNase I (8 U/ml) in RPMI-1640 medium. Single cells and debris were removed from the resulting carcinoma organoid preparation by differential centrifugation. Purified carcinoma organoids were dissociated into single cell suspension in 0.25% trypsin with 0.1% ethylene diaminetetraacetic acid (EDTA) and washed in PBS. Cells (4×10^5 in 20 μl PBS) were injected into the inguinal mammary glands of host mice.

Tumor Response to Doxorubicin and Cisplatin

Mice received 8 mg/kg doxorubicin hydrochloride (in PBS; Sigma-Aldrich, St. Louis, MO, USA) or 10 mg/kg cisplatin (in 10% dimethyl sulfoxide in PBS; MBL International, Woburn, MA, USA) i.p. on days 0, 7, and 14. Control mice were injected with sterile PBS. Tumors were measured 2–3 times a week by caliper, and tumor volumes were calculated as length × width^2/2.

Spinning Disk Confocal Imaging of Live Mice

Details of the microscope design and imaging procedure were previously described (Egeblad et al., 2008). To track cell death, mice were injected i.p. with 50 μl/h propidium iodide (PI; 0.05–0.1 mg/ml; Invitrogen, Grand Island, NY, USA) in sterile PBS. To determine doxorubicin distribution, MMTV-PyMT mice were injected i.v. with AngioSPARK 680 (100 μl of stock solution; PerkinElmer, Waltham, MA, USA) and doxorubicin (8 mg/kg body weight in 200 μl PBS). To determine vascular leakage, mice were injected i.v. with 100 μl sterile PBS containing 1 mg/ml 10 kD Alexa-Fluor-647-conjugated dextran and 1 mg/ml 2 MD rhodamine-conjugated dextran (Invitrogen).

(F) Depletion of MMP9 increases phosphorylation of VE-cadherin in endothelial cells (mean ± SEM, p < 0.0001, Student's t test, 113 vessels from tumors of nine MMTV-Neu;$Mmp9^{+/+}$ mice and 101 vessels from tumors of nine MMTV-Neu;$Mmp9^{-/-}$ mice were examined).

(G) Pericyte coverage is decreased in the absence of MMP9. Double immunofluorescence was used to determine the ratio of αSMA-positive pericytes to CD31-positive endothelial cells (mean ± SEM, p = 0.002, Student's t test, 87 vessels from tumors of ten MMTV-Neu;$Mmp9^{+/+}$ mice and 71 vessels from tumors of nine MMTV-Neu;$Mmp9^{-/-}$ mice were examined).

(H) MMTV-Neu;$Mmp9^{-/-}$ (n = 7 tumors from five mice) tumors respond better to treatment with doxorubicin than do MMTV-Neu;$Mmp9^{+/+}$ tumors (n = 11 tumors from six mice; mean ± SEM, * indicates p < 0.05; Student's t test). Tumors below 256 mm^3 at the beginning of treatment were excluded from the analysis. Also see Figure S4.
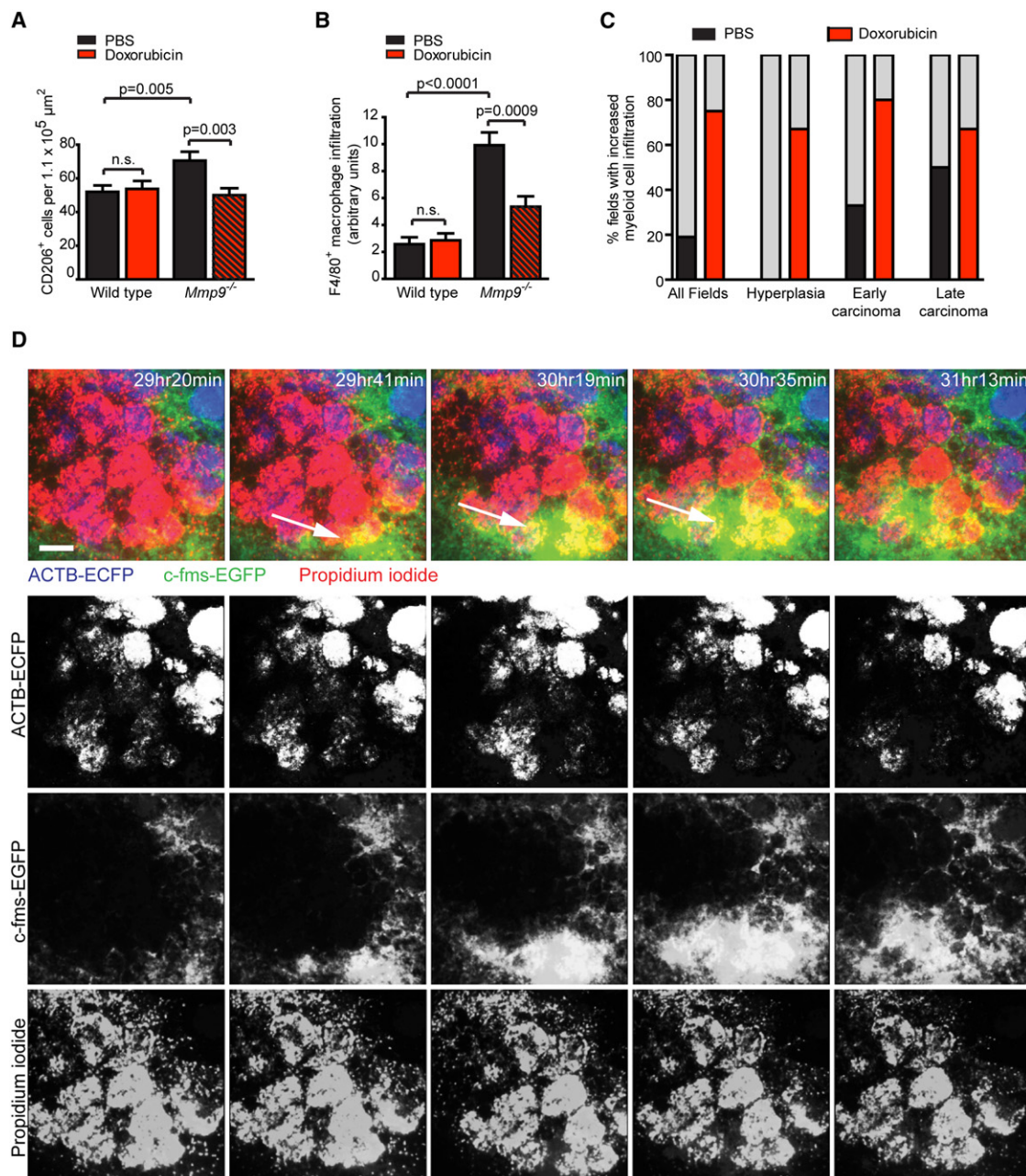
Figure 6. Myeloid Cells Are Recruited to Areas of Tumor Necrosis

(A and B) The infiltration of (A) alternatively activated macrophages (n = 40 FOV from tumors of four mice per condition) and (B) the total macrophage population (n = 22–30 FOV from 4–5 mice per condition) is increased in $Mmp9^{-/-}$ host mice transplanted with MMTV-PyMT tumor cells. The infiltration of these cells decreases 48 hr after doxorubicin treatment (mean ± SEM, n.s. or significant as indicated, Student's t test).

(C) Myeloid cells are recruited to tumors after doxorubicin treatment (12 of 16 movies) as compared to tumors of PBS-treated control mice (3 of 16 movies, p = 0.004, Fisher's exact test; three mice were analyzed per condition).

(D) Dynamics of myeloid cell infiltration (arrow) into an area of necrosis in a doxorubicin-treated MMTV-PyMT;ACTB-ECFP;c-fms-EGFP mouse. Time after treatment is indicated. Scale bar: 100 μm.

Also see Figure S5 and Movies S7, S8, and S9.

Histology and Immunostaining

Paraformaldehyde-fixed, paraffin-embedded sections were stained with Mayer's hematoxylin and eosin. Immunostaining was done with primary antibodies against 7/4 (Cedarlane, Burlington, NC, USA), BrdU and MECA-32 (Developmental Studies Hybridoma Bank, University of Iowa, Iowa City, IA, USA), CCL2, CD206, and F4/80 (AbD Serotec, Raleigh, NC, USA), CCR2 (Novus Biologicals, Littleton, CO, USA), phospho-histone H2AX and phospho-histone H3 (Cell Signaling, Danvers, MA, USA), αSMA (Sigma-Aldrich), CD31 and phospho-VE-cadherin (Abcam, Cambridge, MA, USA), and MMP9 (Rasch et al., 2010). Immunostained slides were quantified by counting
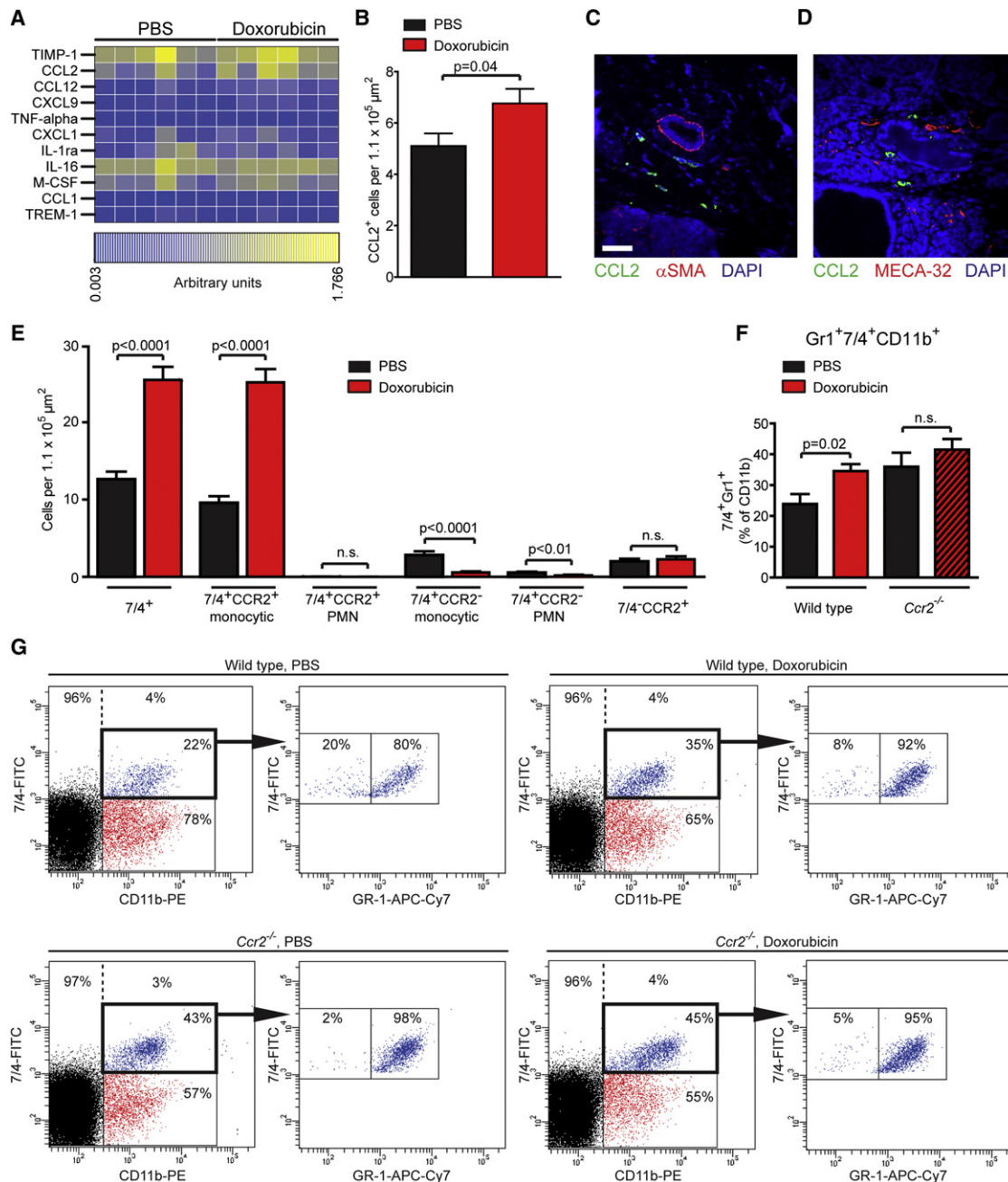
Figure 7. Myeloid Cells Are Recruited to Doxorubicin-treated Tumors through a Stromal CCL2/CCR2 Chemokine/Chemokine Receptor Axis

(A) Protein array identifies CCL2 as the most upregulated chemokine in tumor lysates 48 hr after doxorubicin treatment (p = 0.09 for CCL2 and p = 0.03 for CCL12, Student's t test). Each column represents a tumor from a different mouse.

(B) The number of CCL2-expressing cells increases 48 hr after treatment with doxorubicin (mean ± SEM, p = 0.04, Student's t test; 80 FOV from six PBS-treated and 66 FOV from six doxorubicin-treated mice were analyzed).

(C and D) Endothelial cells, pericytes, and fibroblasts do not express CCL2. Tumor tissue from MTMV-PyMT mice isolated 48 hr after treatment with doxorubicin was immunostained for CCL2 and (C) α-smooth muscle actin (αSMA, a pericyte, and fibroblast marker) or (D) MECA-32 (an endothelial cell marker). More than 300 αSMA or MECA-32 positive cells from PBS and doxorubicin-treated tumors were observed, and none were positive for CCL2. Scale bar: 50 μm.

(E) Doxorubicin treatment results in infiltration of $7/4^+CCR2^+$ cells with monocytic but not polymorphonuclear (PMN) morphology. Double immunostaining for CCR2 and 7/4 with scoring of nuclear morphology (mean ± SEM, Student's t test, significance levels as indicted; 104 FOV from four PBS-treated and 113 FOV from five doxorubicin-treated mice).

(F) Doxorubicin results in CCR2-dependent myeloid cell infiltration. The percentage of $Gr1^+7/4^+$ of all $CD11b^+$ myeloid cells in tumors was determined by flow cytometry (mean ± SEM, significance levels as indicated, Student's t test, n = 10–11 mice).

(G) FACS plots with indication of the percentages of the gated cell populations from representative tumors.
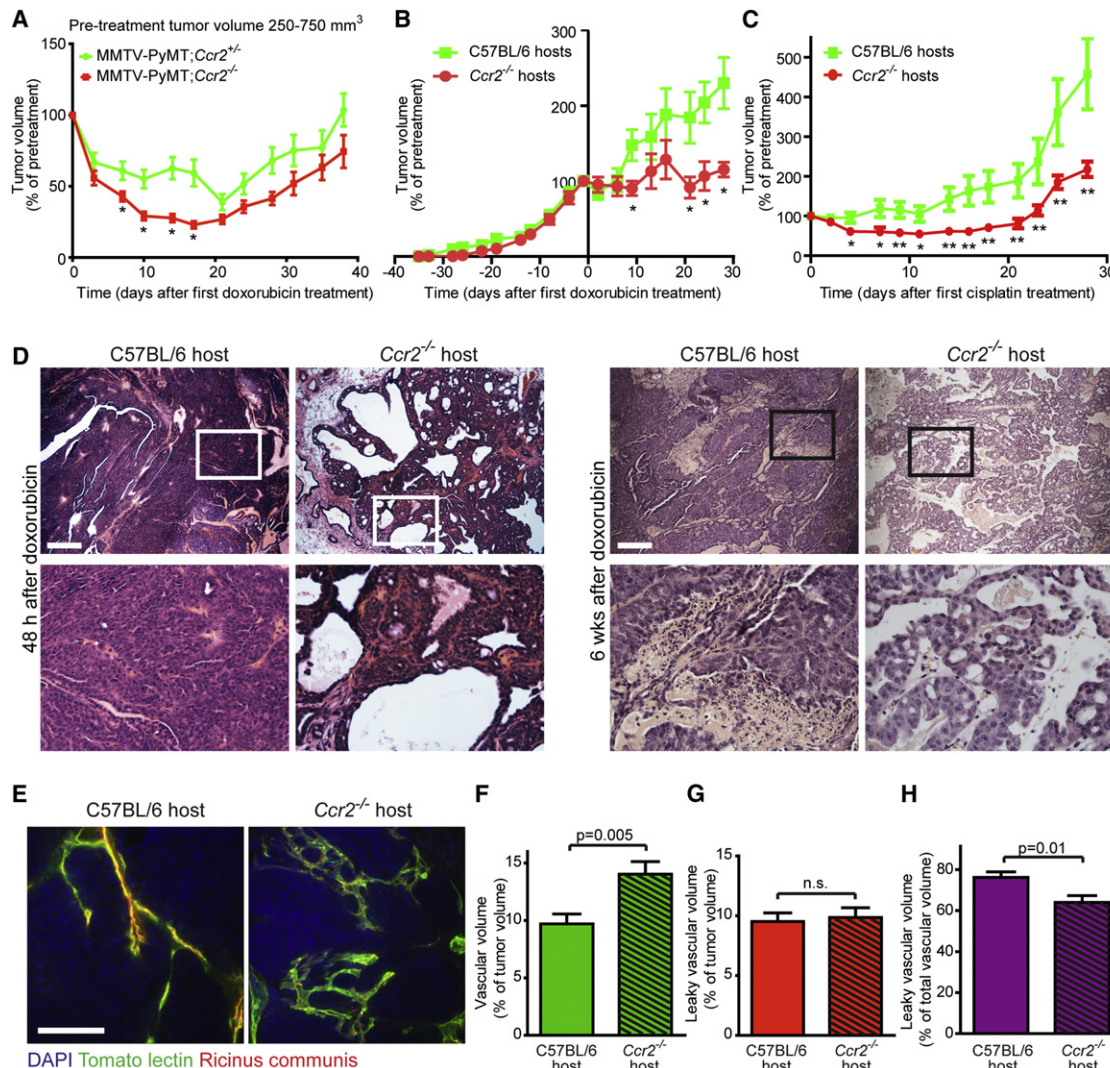
Also see Figure S6.

Figure 8. Host CCR2 Regulates Response to Doxorubicin

(A) Tumors in MMTV-PyMT;*Ccr2*$^{-/-}$ (26 tumors from ten mice) respond better to doxorubicin than those in MMTV-PyMT;*Ccr2*$^{+/-}$ (15 tumors from eight mice). Results for tumors with a pretreatment volume of 250–750 mm^3 (mean ± SEM, * indicates p < 0.05, Student's t test).

(B) Tumors in *Ccr2*$^{-/-}$ host mice respond better to doxorubicin than those in C57BL/6 hosts. Two cohorts were treated with doxorubicin and showed similar results. The results of one cohort are shown (mean ± SEM, * indicates p < 0.05, Student's t test; eight tumors in 6–8 hosts were analyzed per condition; one *Ccr2*$^{-/-}$ and two C57BL/6 hosts were euthanized on days 13–16 due to poor health).

(C) Tumors in *Ccr2*$^{-/-}$ hosts respond better to cisplatin than those in C57BL/6 hosts (mean ± SEM, * indicates p < 0.05, ** indicates p < 0.01, Student's t test, n = 22–24 tumors in 11–12 hosts).

(D) Tumors in *Ccr2*$^{-/-}$ hosts are more cystic and contain fewer cancer cells acutely (48 hr) after doxorubicin treatment. Relapsed tumors (six weeks after treatment) in *Ccr2*$^{-/-}$ hosts are low-grade with decreased cellularity and necrosis (p = 0.005, Fisher's exact test; ten low-grade and five high-grade tumors in *Ccr2*$^{-/-}$ hosts versus one low-grade and eleven high-grade tumors in C57BL/6 hosts). Scale bar: 100 μm.

(E) Vascular structure of tumors in *Ccr2*$^{-/-}$ and C57BL/6 hosts analyzed by perfusion with FITC-conjugated tomato lectin (green) and rhodamine-conjugated *Ricinus communis* agglutinin I (red). Nuclei are stained with 4′,6-diamidino-2-phenylindole (DAPI). Scale bar: 100 μm.

(F) Vascular volume is increased in tumors in *Ccr2*$^{-/-}$ hosts compared to C57BL/6 wild-type hosts as determined by perfusion with tomato lectin (mean ± SEM, p = 0.005, Student's t test; analysis of 12 tumors from six mice per genotype and 5–10 fields of view per tumor).

(G) The total volume of leaky vasculature does not differ between tumors in *Ccr2*$^{-/-}$ and C57BL/6 hosts (mean ± SEM; n.s., Student's t test; analysis of 12 tumors from six mice per genotype and 5–10 FOV per tumor).

(H) Relative leaky vasculature is decreased in tumors of *Ccr2*$^{-/-}$ hosts compared to C57BL/6 hosts as determined by the percentage of the vasculature that is positive for *Ricinus communis* agglutinin I (mean ± SEM, p = 0.01, Student's t test; analysis of 12 tumors from six mice per genotype and 5–10 FOV per tumor). Also see Figure S7.

(for 7/4, BrdU, CCL2, CCR2, CD206, phospho-histone H2AX, and phospho-histone H3) or by fluorescence intensity with Volocity software (PerkinElmer; for F4/80, phospho-VE-cadherin, αSMA, and CD31).

In Vitro Drug Sensitivity

Tumor lesions were isolated from MMTV-PyMT;ACTB-ECFP mice using a fluorescent dissection microscope, and primary mammary organoids were

isolated from different tumor stages and cultured in Growth Factor Reduced Matrigel (BD Biosciences, San Diego, CA, USA). To determine doxorubicin sensitivity, treatment of tumor organoids was started 72 hr after isolation. To determine lapatinib sensitivity, single cell suspensions were generated from tumor organoids, isolated as described previously, grown to subconfluence, re-seeded, and treated with lapatinib (Selleck Chemicals, LLC, Houston, TX, USA). Cell viability was measured 48 hr after the addition of drugs using the CellTiter 96 Aqueous One Solution Cell Proliferation Assay (Promega, Madison, WI, USA).

For further experimental details, see Supplemental Experimental Procedures.

SUPPLEMENTAL INFORMATION

ACKNOWLEDGMENTS

REFERENCES

Ahn, G.O., Tseng, D., Liao, C.H., Dorie, M.J., Czechowicz, A., and Brown, J.M. (2010). Inhibition of Mac-1 (CD11b/CD18) enhances tumor response to radiation by reducing myeloid cell recruitment. Proc. Natl. Acad. Sci. USA 107, 8363–8368.

Campiglio, M., Somenzi, G., Olgiati, C., Beretta, G., Balsari, A., Zaffaroni, N., Valagussa, P., and Ménard, S. (2003). Role of proliferation in HER2 status predicted response to doxorubicin. Int. J. Cancer 105, 568–573.

Coussens, L.M., Fingleton, B., and Matrisian, L.M. (2002). Matrix metalloproteinase inhibitors and cancer: trials and tribulations. Science 295, 2387–2392.

Dean, M., Fojo, T., and Bates, S. (2005). Tumour stem cells and drug resistance. Nat. Rev. Cancer 5, 275–284.

Denardo, D.G., Brennan, D.J., Rexhepaj, E., Ruffell, B., Shiao, S.L., Madden, S.F., Gallagher, W.M., Wadhwani, N., Keil, S.D., Junaid, S.A., et al. (2011). Leukocyte complexity predicts breast cancer survival and functionally regulates response to chemotherapy. Cancer Discov. 1, 54–67.

Dive, C., Gregory, C.D., Phipps, D.J., Evans, D.L., Milner, A.E., and Wyllie, A.H. (1992). Analysis and discrimination of necrosis and apoptosis (programmed cell death) by multiparameter flow cytometry. Biochim. Biophys. Acta 1133, 275–285.

Ebrahem, Q., Chaurasia, S.S., Vasanji, A., Qi, J.H., Klenotic, P.A., Cutler, A., Asosingh, K., Erzurum, S., and Anand-Apte, B. (2010). Cross-talk between vascular endothelial growth factor and matrix metalloproteinases in the induction of neovascularization in vivo. Am. J. Pathol. 176, 496–503.

Egeblad, M., Ewald, A.J., Askautrud, H.A., Truitt, M.L., Welm, B.E., Bainbridge, E., Peeters, G., Krummel, M.F., and Werb, Z. (2008). Visualizing stromal cell dynamics in different tumor microenvironments by spinning disk confocal microscopy. Dis. Model Mech. 1, 155–167.

Egeblad, M., Nakasone, E.S., and Werb, Z. (2010). Tumors as organs: complex tissues that interface with the entire organism. Dev. Cell 18, 884–901.

Fujimoto, H., Sangai, T., Ishii, G., Ikehara, A., Nagashima, T., Miyazaki, M., and Ochiai, A. (2009). Stromal MCP-1 in mammary tumors induces tumor-associated macrophage infiltration and contributes to tumor progression. Int. J. Cancer 125, 1276–1284.

Gavard, J. (2009). Breaking the VE-cadherin bonds. FEBS Lett. 583, 1–6.

Gilbert, L.A., and Hemann, M.T. (2010). DNA damage-mediated induction of a chemoresistant niche. Cell 143, 355–366.

Goel, S., Duda, D.G., Xu, L., Munn, L.L., Boucher, Y., Fukumura, D., and Jain, R.K. (2011). Normalization of the vasculature for treatment of cancer and other diseases. Physiol. Rev. 91, 1071–1121.

Gong, Y., Hart, E., Shchurin, A., and Hoover-Plow, J. (2008). Inflammatory macrophage migration requires MMP-9 activation by plasminogen in mice. J. Clin. Invest. 118, 3012–3024.

Greene, R.F., Collins, J.M., Jenkins, J.F., Speyer, J.L., and Myers, C.E. (1983). Plasma pharmacokinetics of adriamycin and adriamycinol: implications for the design of in vitro experiments and treatment protocols. Cancer Res. 43, 3417–3421.

Guerriero, J.L., Ditsworth, D., Catanzaro, J.M., Sabino, G., Furie, M.B., Kew, R.R., Crawford, H.C., and Zong, W.X. (2011). DNA alkylating therapy induces tumor regression through an HMGB1-mediated activation of innate immunity. J. Immunol. 186, 3517–3526.

Hadjantonakis, A.-K., and Papaioannou, V.E. (2004). Dynamic in vivo imaging and cell tracking using a histone fluorescent protein fusion in mice. BMC Biotechnol. 4, 33.

Hagendoorn, J., Tong, R., Fukumura, D., Lin, Q., Lobo, J., Padera, T.P., Xu, L., Kucherlapati, R., and Jain, R.K. (2006). Onset of abnormal blood and lymphatic vessel function and interstitial hypertension in early stages of carcinogenesis. Cancer Res. 66, 3360–3364.

Herschkowitz, J.I., Simin, K., Weigman, V.J., Mikaelian, I., Usary, J., Hu, Z., Rasmussen, K.E., Jones, L.P., Assefnia, S., Chandrasekharan, S., et al. (2007). Identification of conserved gene expression features between murine mammary carcinoma models and human breast tumors. Genome Biol. 8, R76.

Johnson, J.I., Decker, S., Zaharevitz, D., Rubinstein, L.V., Venditti, J.M., Schepartz, S., Kalyandrug, S., Christian, M., Arbuck, S., Hollingshead, M., and Sausville, E.A. (2001). Relationships between drug activity in NCI preclinical in vitro and in vivo models and early clinical trials. Br. J. Cancer 84, 1424–1431.

Lin, E.Y., Jones, J.G., Li, P., Zhu, L., Whitney, K.D., Muller, W.J., and Pollard, J.W. (2003). Progression to malignancy in the polyoma middle T oncoprotein mouse breast cancer model provides a reliable model for human diseases. Am. J. Pathol. 163, 2113–2126.

Loberg, R.D., Ying, C., Craig, M., Day, L.L., Sargent, E., Neeley, C., Wojno, K., Snyder, L.A., Yan, L., and Pienta, K.J. (2007). Targeting CCL2 with systemic delivery of neutralizing antibodies induces prostate cancer tumor regression in vivo. Cancer Res. 67, 9417–9424.

Loeffler, M., Krüger, J.A., Niethammer, A.G., and Reisfeld, R.A. (2006). Targeting tumor-associated fibroblasts improves cancer chemotherapy by increasing intratumoral drug uptake. J. Clin. Invest. 116, 1955–1962.

Martin, M.D., Carter, K.J., Jean-Philippe, S.R., Chang, M., Mobashery, S., Thiolloy, S., Lynch, C.C., Matrisian, L.M., and Fingleton, B. (2008). Effect of ablation or inhibition of stromal matrix metalloproteinase-9 on lung metastasis in a breast cancer model is dependent on genetic background. Cancer Res. 68, 6251–6259.

Meads, M.B., Gatenby, R.A., and Dalton, W.S. (2009). Environment-mediated drug resistance: a major contributor to minimal residual disease. Nat. Rev. Cancer 9, 665–674.

Minchinton, A.I., and Tannock, I.F. (2006). Drug penetration in solid tumours. Nat. Rev. Cancer 6, 583–592.

Murdoch, C., Giannoudis, A., and Lewis, C.E. (2004). Mechanisms regulating the recruitment of macrophages into hypoxic areas of tumors and other ischemic tissues. Blood 104, 2224–2234.

Netti, P.A., Hamberg, L.M., Babich, J.W., Kierstead, D., Graham, W., Hunter, G.J., Wolf, G.L., Fischman, A., Boucher, Y., and Jain, R.K. (1999). Enhancement of fluid filtration across tumor vessels: implication for delivery of macromolecules. Proc. Natl. Acad. Sci. USA 96, 3137–3142.

Obeid, M., Tesniere, A., Ghiringhelli, F., Fimia, G.M., Apetoh, L., Perfettini, J.L., Castedo, M., Mignot, G., Panaretakis, T., Casares, N., et al. (2007). Calreticulin exposure dictates the immunogenicity of cancer cell death. Nat. Med. 13, 54–61.

Olive, K.P., Jacobetz, M.A., Davidson, C.J., Gopinathan, A., McIntyre, D., Honess, D., Madhu, B., Goldgraben, M.A., Caldwell, M.E., Allard, D., et al. (2009). Inhibition of Hedgehog signaling enhances delivery of chemotherapy in a mouse model of pancreatic cancer. Science 324, 1457–1461.

Pahler, J.C., Tazzyman, S., Erez, N., Chen, Y.Y., Murdoch, C., Nozawa, H., Lewis, C.E., and Hanahan, D. (2008). Plasticity in tumor-promoting inflammation: impairment of macrophage recruitment evokes a compensatory neutrophil response. Neoplasia 10, 329–340.

Priceman, S.J., Sung, J.L., Shaposhnik, Z., Burton, J.B., Torres-Collado, A.X., Moughon, D.L., Johnson, M., Lusis, A.J., Cohen, D.A., Iruela-Arispe, M.L., and Wu, L. (2010). Targeting distinct tumor-infiltrating myeloid cells by inhibiting CSF-1 receptor: combating tumor evasion of antiangiogenic therapy. Blood 115, 1461–1471.

Rasch, M.G., Lund, I.K., Illemann, M., Høyer-Hansen, G., and Gårdsvoll, H. (2010). Purification and characterization of recombinant full-length and protease domain of murine MMP-9 expressed in Drosophila S2 cells. Protein Expr. Purif. 72, 87–94.

Rottenberg, S., Pajic, M., and Jonkers, J. (2010). Studying drug resistance using genetically engineered mouse models for breast cancer. Methods Mol. Biol. 596, 33–45.

Rouzier, R., Perou, C.M., Symmans, W.F., Ibrahim, N., Cristofanilli, M., Anderson, K., Hess, K.R., Stec, J., Ayers, M., Wagner, P., et al. (2005). Breast cancer molecular subtypes respond differently to preoperative chemotherapy. Clin. Cancer Res. 11, 5678–5685.

Sadik, C.D., Kim, N.D., and Luster, A.D. (2011). Neutrophils cascading their way to inflammation. Trends Immunol. 32, 452–460.

Shree, T., Olson, O.C., Elie, B.T., Kester, J.C., Garfall, A.L., Simpson, K., Bell-McGuinn, K.M., Zabor, E.C., Brogi, E., and Joyce, J.A. (2011). Macrophages and cathepsin proteases blunt chemotherapeutic response in breast cancer. Genes Dev. 25, 2465–2479.

Sounni, N.E., Dehne, K., van Kempen, L., Egeblad, M., Affara, N.I., Cuevas, I., Wiesen, J., Junankar, S., Korets, L., Lee, J., et al. (2010). Stromal regulation of vessel stability by MMP14 and TGFbeta. Dis. Model Mech. 3, 317–332.

Thurston, G., Suri, C., Smith, K., McClain, J., Sato, T.N., Yancopoulos, G.D., and McDonald, D.M. (1999). Leakage-resistant blood vessels in mice transgenically overexpressing angiopoietin-1. Science 286, 2511–2514.

Tsou, C.L., Peters, W., Si, Y., Slaymaker, S., Aslanian, A.M., Weisberg, S.P., Mack, M., and Charo, I.F. (2007). Critical roles for CCR2 and MCP-3 in monocyte mobilization from bone marrow and recruitment to inflammatory sites. J. Clin. Invest. 117, 902–909.

Vu, T.H., Shipley, J.M., Bergers, G., Berger, J.E., Helms, J.A., Hanahan, D., Shapiro, S.D., Senior, R.M., and Werb, Z. (1998). MMP-9/gelatinase B is a key regulator of growth plate angiogenesis and apoptosis of hypertrophic chondrocytes. Cell 93, 411–422.

Welford, A.F., Biziato, D., Coffelt, S.B., Nucera, S., Fisher, M., Pucci, F., Di Serio, C., Naldini, L., De Palma, M., Tozer, G.M., and Lewis, C.E. (2011). TIE2-expressing macrophages limit the therapeutic efficacy of the vascular-disrupting agent combretastatin A4 phosphate in mice. J. Clin. Invest. 121, 1969–1973.

Yu, Q., and Stamenkovic, I. (2000). Cell surface-localized matrix metalloproteinase-9 proteolytically activates TGF-beta and promotes tumor invasion and angiogenesis. Genes Dev. 14, 163–176.

Zhang, J., Lu, Y., and Pienta, K.J. (2010). Multiple roles of chemokine (C-C motif) ligand 2 in promoting prostate cancer growth. J. Natl. Cancer Inst. 102, 522–528.